RESEARCH ARTICLE

Figures and figure supplements

Exploratory mass cytometry analysis reveals immunophenotypes of cancer treatment-related pneumonitis

Toyoshi Yanagihara and Kentaro Hata *et al*.

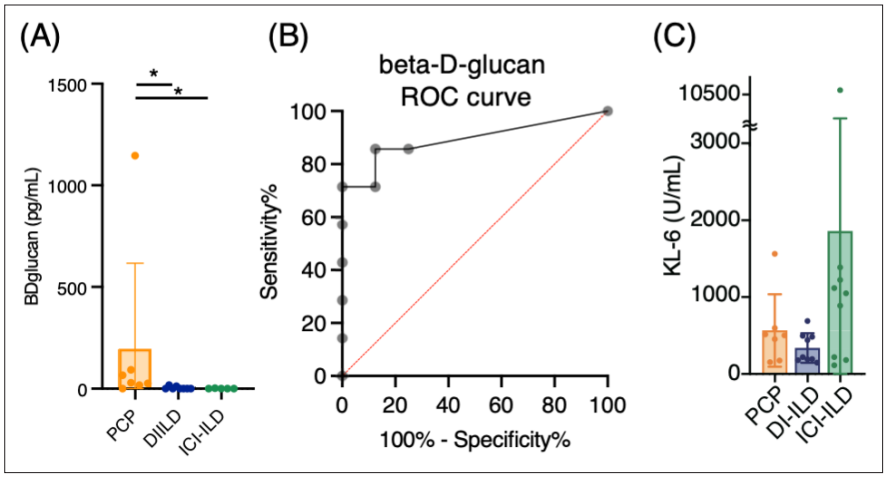

Figure 1. Serum levels of β-D-glucan and KL-6 from patients with *Pneumocystis jirovecii* pneumonia (PCP), cytotoxic drug-related interstitial lung disease (DI-ILD), and immune-checkpoint inhibitor-related ILD (ICI-ILD). (**A**) Serum levels of β-D-glucan from patients with PCP, DI-ILD, and ICI-ILD. (**B**) A receiver operating characteristic (ROC) curve was constructed to evaluate the diagnostic utility of β-D-glucan for PCP, with values from the DI-ILD group used as a reference. The area under the curve was determined to be 0.8929. (**C**) Serum levels of KL-6.

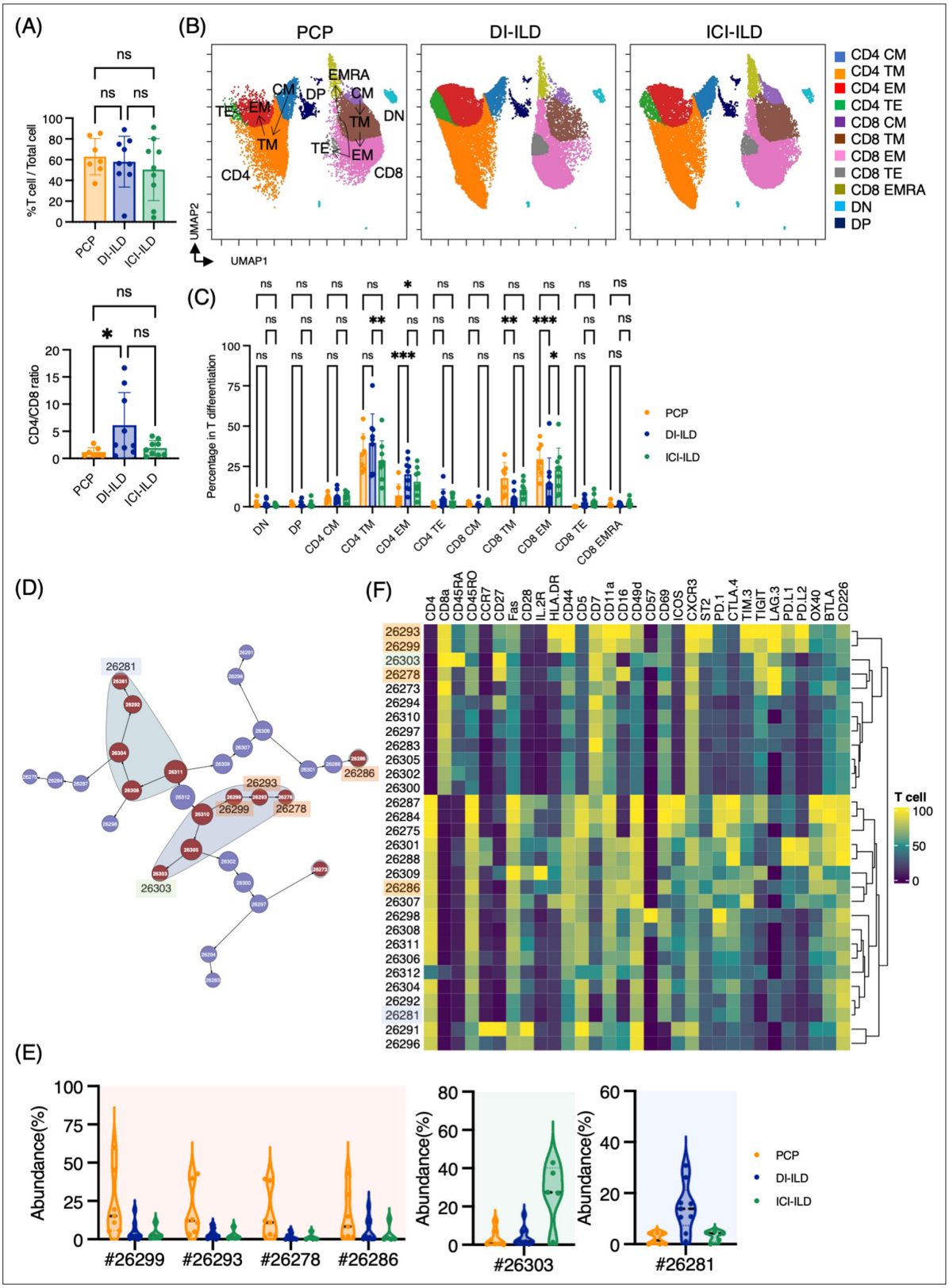

Figure 2. Characterization of T cell subsets in bronchoalveolar lavage fluid (BALF) from patients with *Pneumocystis jirovecii* pneumonia (PCP), cytotoxic drug-related interstitial lung disease (DI-ILD), and immune-checkpoint inhibitor-related ILD (ICI-ILD). (**A**) Percentage of T cells (defined as $CD2^{+}CD3^{+}$) in $CD45^{+}$ BALF cells and CD4/CD8 ratio in T cells from patients with PCP, DI-ILD, and ICI-ILD. (**B**) Uniform Manifold Approximation and Projection (UMAP) of concatenated samples visualizing the distribution of T cell subpopulations. Central memory (CM) T cells were defined by $CCR7^{+}$ $CD45RO^{+}$

Figure 2 continued on next page

Figure 2 continued

CD28^{+} Fas^{+}, transitional memory (TM) by CCR7^{-} CD45RO^{+} CD28^{+} Fas^{+}, effector memory (EM) by CCR7^{-} CD45RO^{+} CD28^{-} Fas^{+}, terminal effector (TE) by CCR7^{-} CD45RO$^{+/-}$ Fas^{-}, and effector memory RA (EMRA) by CCR7^{-} CD45RO^{-} CD45RA^{+} Fas$^{+/-}$. Arrows indicate the trajectory of T cell differentiation. DN: CD4^{-} CD8^{-} double negative; DP: CD4^{+} CD8^{+} double positive. (**C**) Percentage of T cell subpopulations. (**D**) Citrus network tree visualizing the hierarchical relationship of each marker between identified T cell populations gated by CD45^{+}CD2^{+} CD3^{+} from PCP (n = 7), DI-ILD (n = 9), and ICI-ILD (n = 5). Clusters with significant differences are represented in red, and those without significant differences in blue. Circle size reflects the number of cells within a given cluster. (**E**) Citrus-generated violin plots for six representative and differentially regulated populations. Each cluster number (#) corresponds to the number shown in panel (**D**). (**F**) Heatmap demonstrates the expression of various markers in different clusters of T cells, as identified through the Citrus analysis. All differences in abundance were significant at a false discovery rate < 0.01.

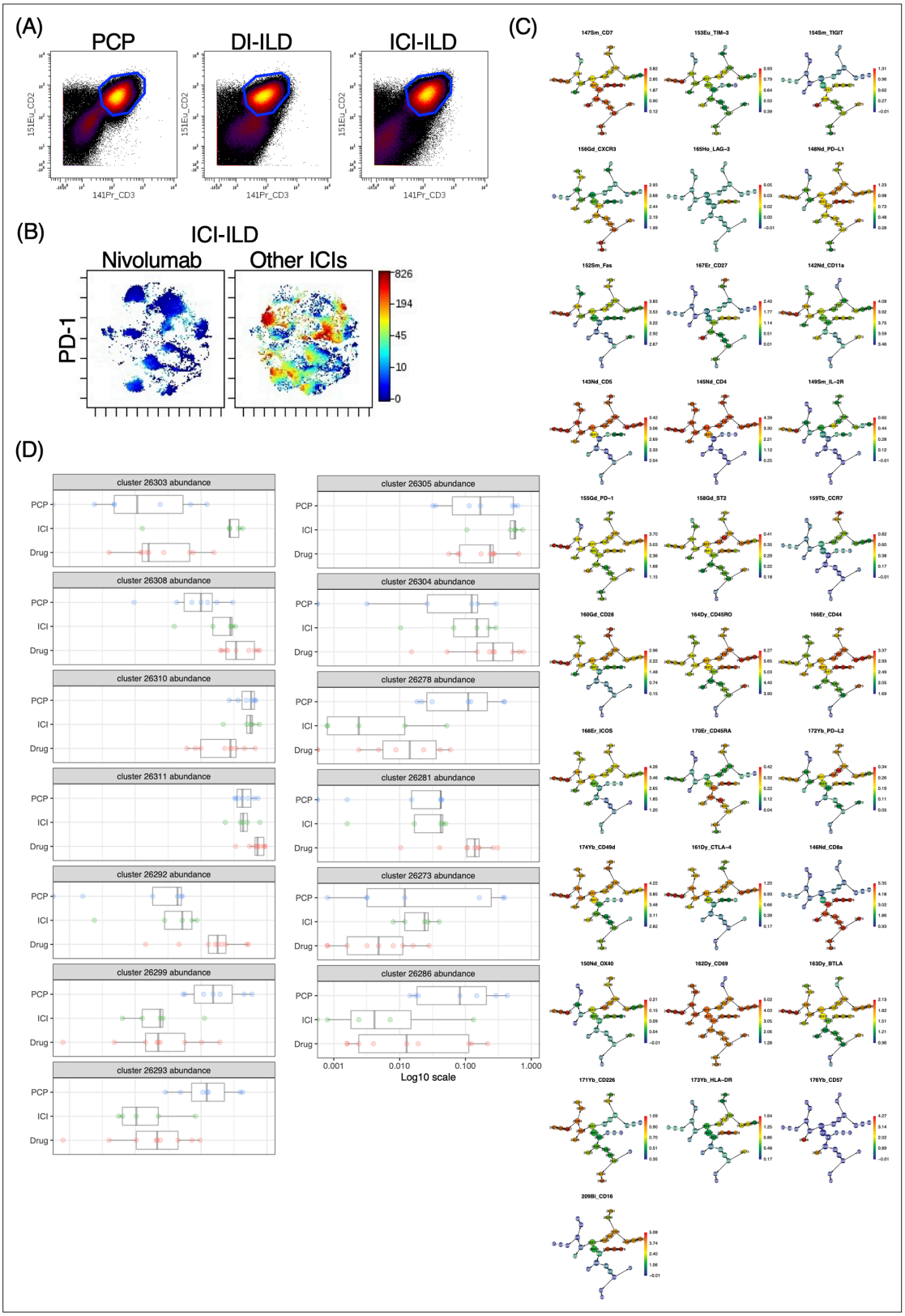

Figure 2—figure supplement 1. A T cell gate ($CD2^{+}CD3^{+}$) and Citrus analysis of T cell populations in bronchoalveolar lavage fluid (BALF) cells from *Pneumocystis jirovecii* pneumonia (PCP), cytotoxic drug-related interstitial lung disease (DI-ILD), and immune-checkpoint inhibitor-related ILD (ICI-ILD). (**A**) Representative dot plots demonstrating the gating strategy for identification of T cell populations within BALF samples from patients with Pneumocystis jirovecii pneumonia (PCP), drug-induced interstitial lung disease (DI-ILD), and immune checkpoint inhibitor-induced lung disease (ICI-ILD).

Figure 2—figure supplement 1 continued on next page

Figure 2—figure supplement 1 continued

(**B**) Density plots comparing the expression of programmed death-ligand 1 (PD-1) on T cells from patients treated with Nivolumab versus other ICIs. (**C**) Citrus analysis of T cell populations with each surface marker. (**D**) Box plots depicting the abundance of distinct T cell clusters identified across different patient groups.

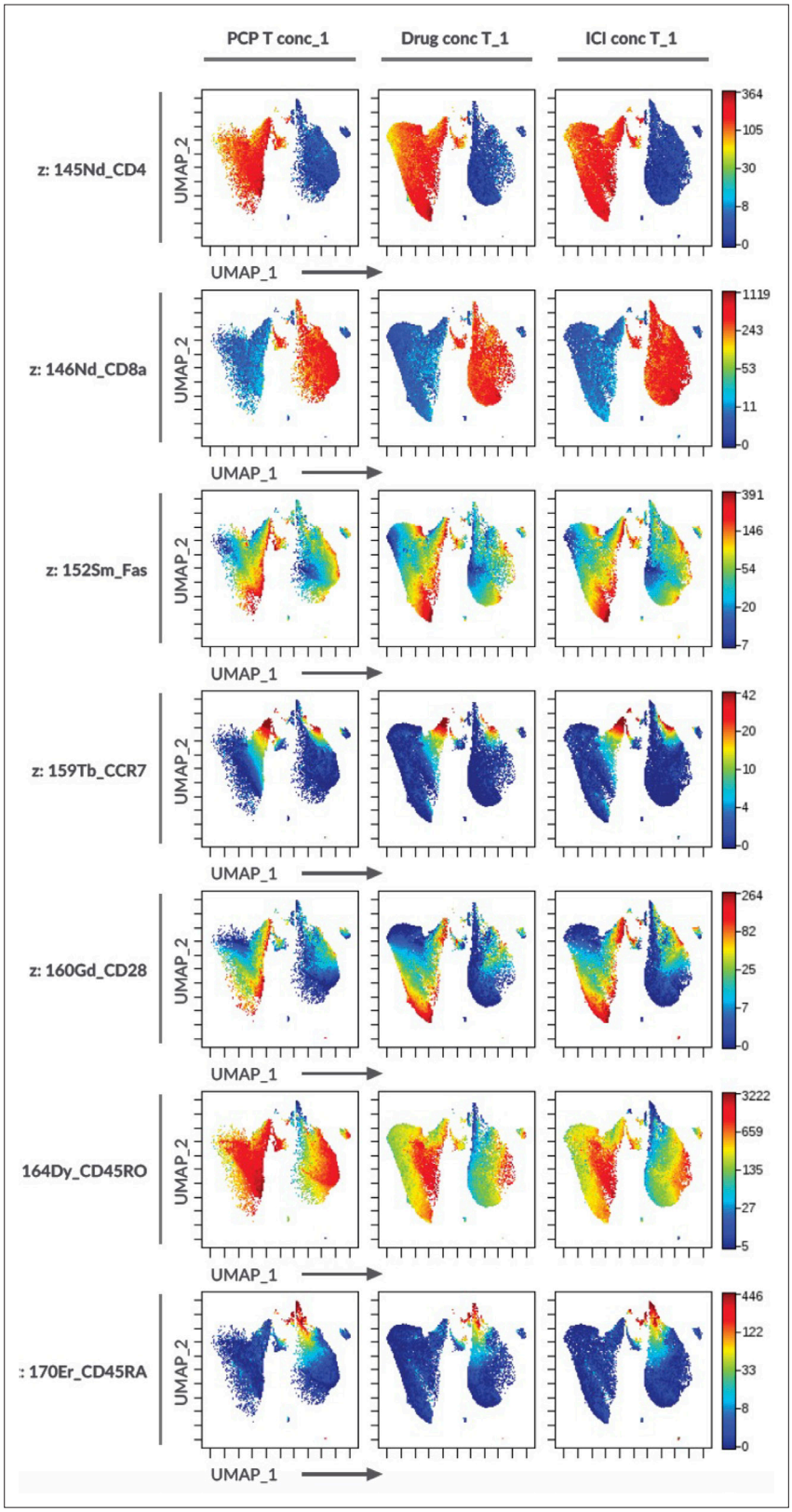

Figure 2—figure supplement 2. T cell marker expression on the Uniform Manifold Approximation and Projection (UMAP) in ***Figure 2B***.

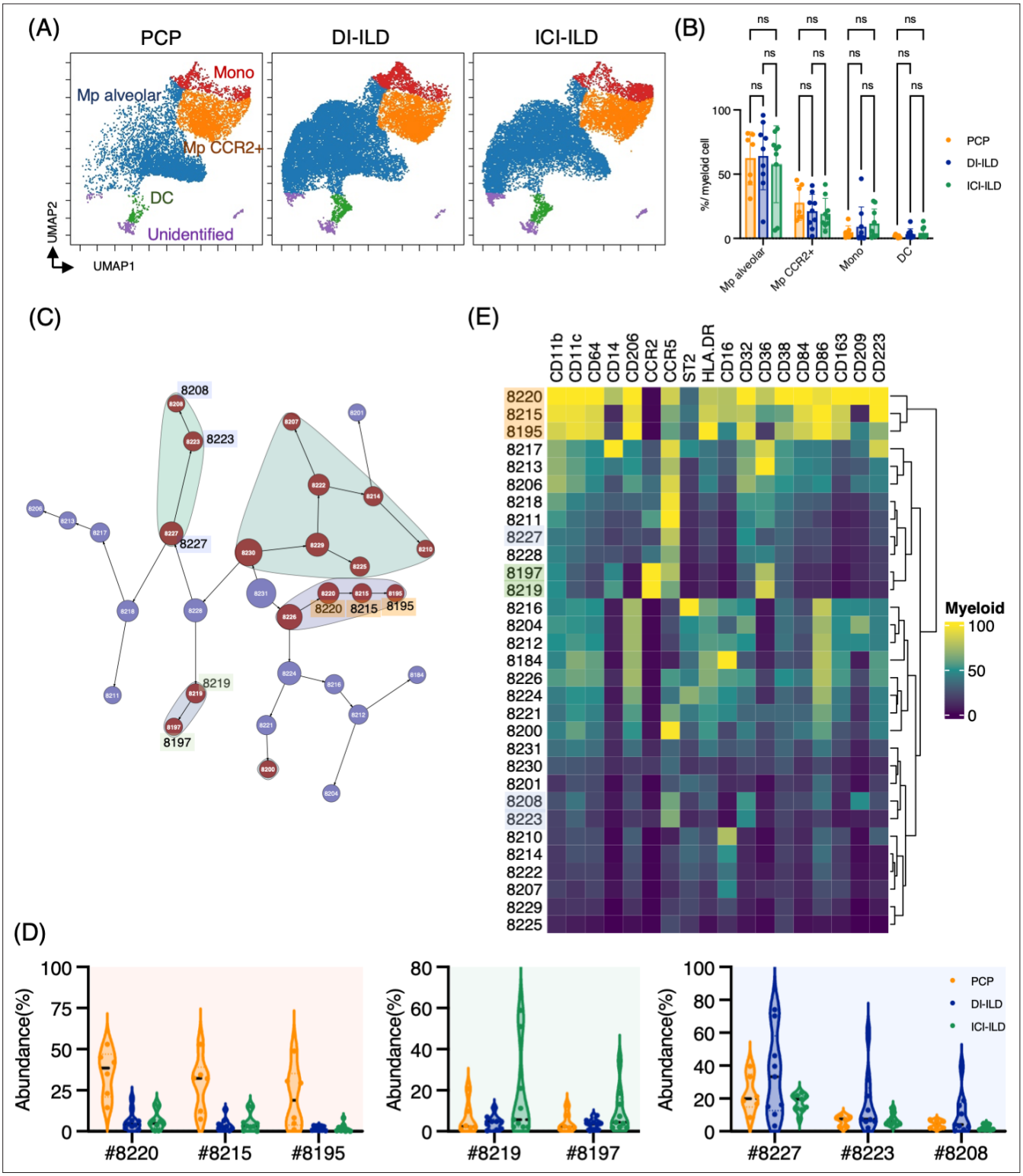

Figure 3. Characterization of myeloid cell subsets in bronchoalveolar lavage fluid (BALF) from patients with *Pneumocystis jirovecii* pneumonia (PCP), cytotoxic drug-related interstitial lung disease (DI-ILD), and immune-checkpoint inhibitor-related ILD (ICI-ILD). (**A**) Uniform Manifold Approximation and Projection (UMAP) of concatenated samples visualizing the distribution of myeloid cell subpopulations in $CD3^-$ $CD11b^+$ $CD11c^+$ gated myeloid cells in BALF from patients with PCP, DI-ILD, and ICI-ILD. Monocytes were defined by $CD64^+$ $CD14^+$, $CCR2^+$ macrophages (Mp) by $CD64^+$ $CD14^-$ $CCR2^+$, alveolar Mp by $CD64^+$ $CD14^-CCR2^-$ $CD206^+$, dendritic cells (DC) by $CD64^-CD14^-CD206^-CD11c^+$ $HLA\text{-}DR^+$, and unidentified subsets by $CD64^-$ $CD11b^{+/-}$ $CD11c^{+/-}$ $CD14^-$ $CD206^-$. (**B**) Percentage of myeloid cell subpopulations in PCP (n = 7), DI-ILD (n = 9), and ICI-ILD (n = 9). Dot plots represent individual samples.

Figure 3 continued on next page

Figure 3 continued

(**C**) Citrus network tree visualizing the hierarchical relationship of each marker between identified myeloid cell populations gated by $CD45^+$ $CD3^-$ $CD11b^+$ $CD11c^+$ from PCP (n = 6), DI-ILD (n = 9), and ICI-ILD (n = 9). Clusters with significant differences are represented in red, and those without significant differences in blue. Circle size reflects the number of cells within a given cluster. (**D**) Citrus-generated violin plots for six representative and differentially regulated populations. Each cluster number (#) corresponds to the number shown in panel (**C**). All differences in abundance were significant at a false discovery rate < 0.01. (**E**) Heatmap demonstrates the expression of various markers in different clusters of myeloid cells, as identified through the Citrus analysis.

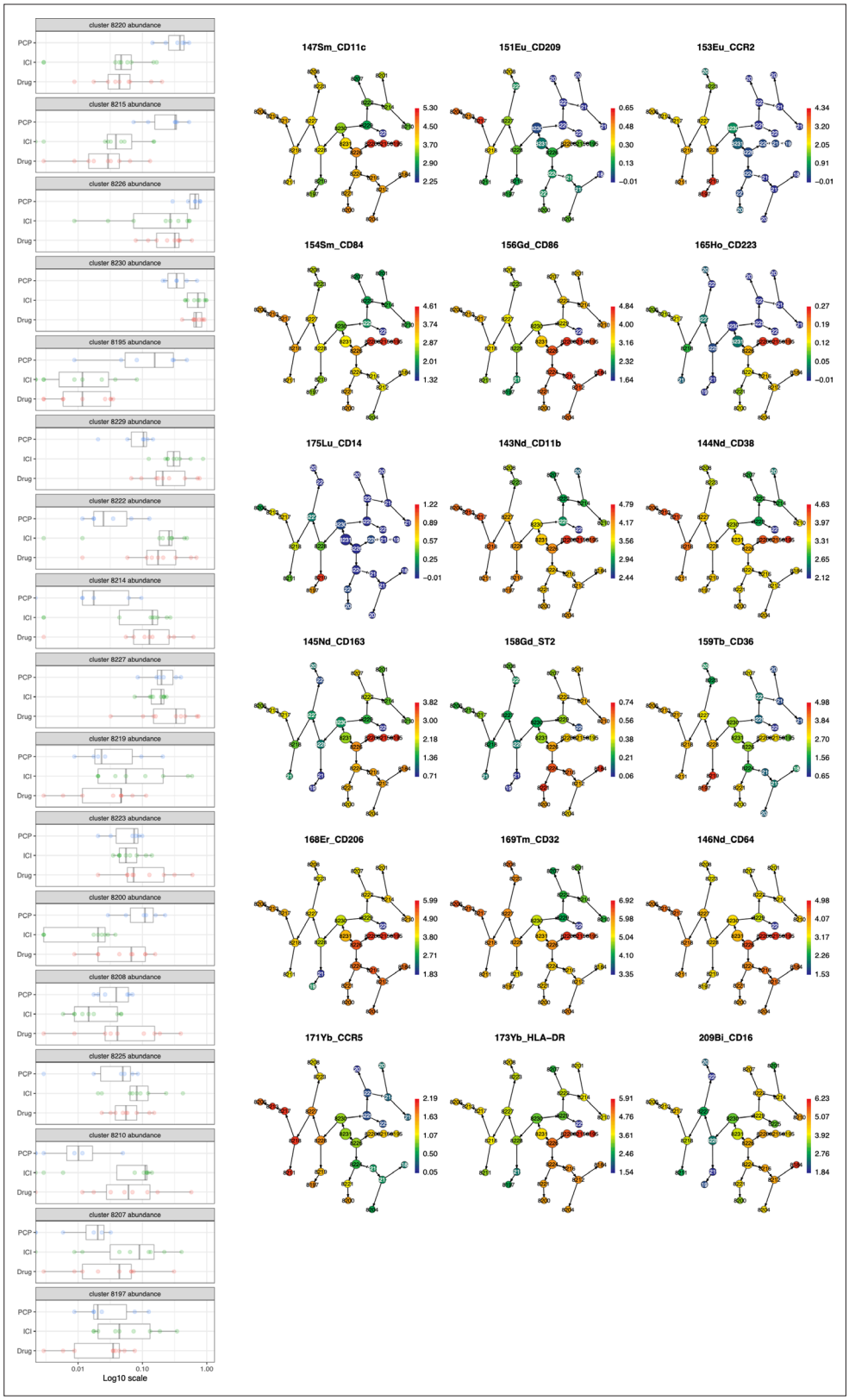

Figure 3—figure supplement 1. The Citrus analysis of myeloid cell populations in bronchoalveolar lavage fluid (BALF) cells from *Pneumocystis jirovecii* pneumonia (PCP), cytotoxic drug-related interstitial lung disease (DI-ILD), and immune-checkpoint inhibitor-related ILD (ICI-ILD).

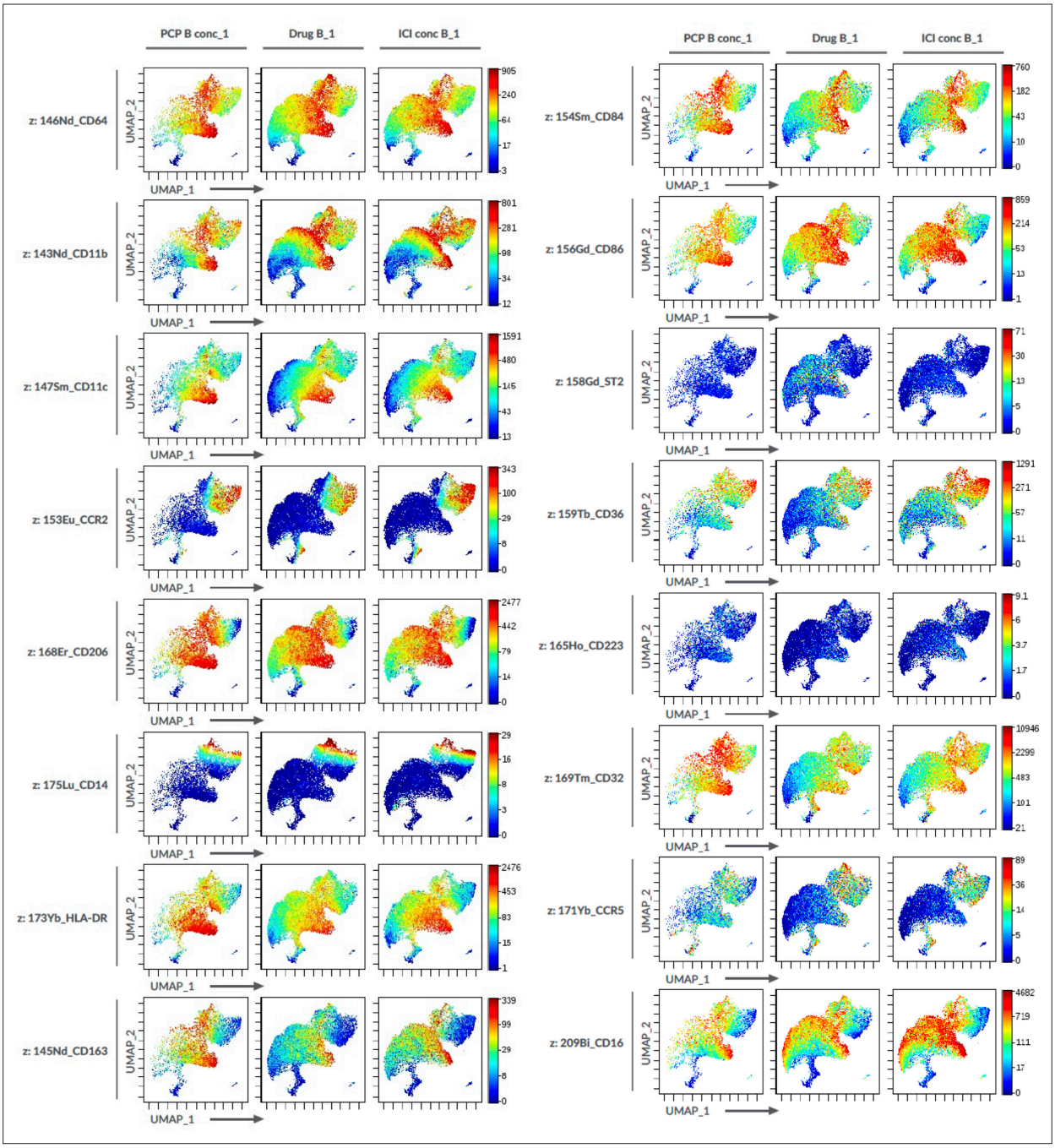

Figure 3—figure supplement 2. Myeloid cell marker expression on the Uniform Manifold Approximation and Projection (UMAP) in ***Figure 3A***.

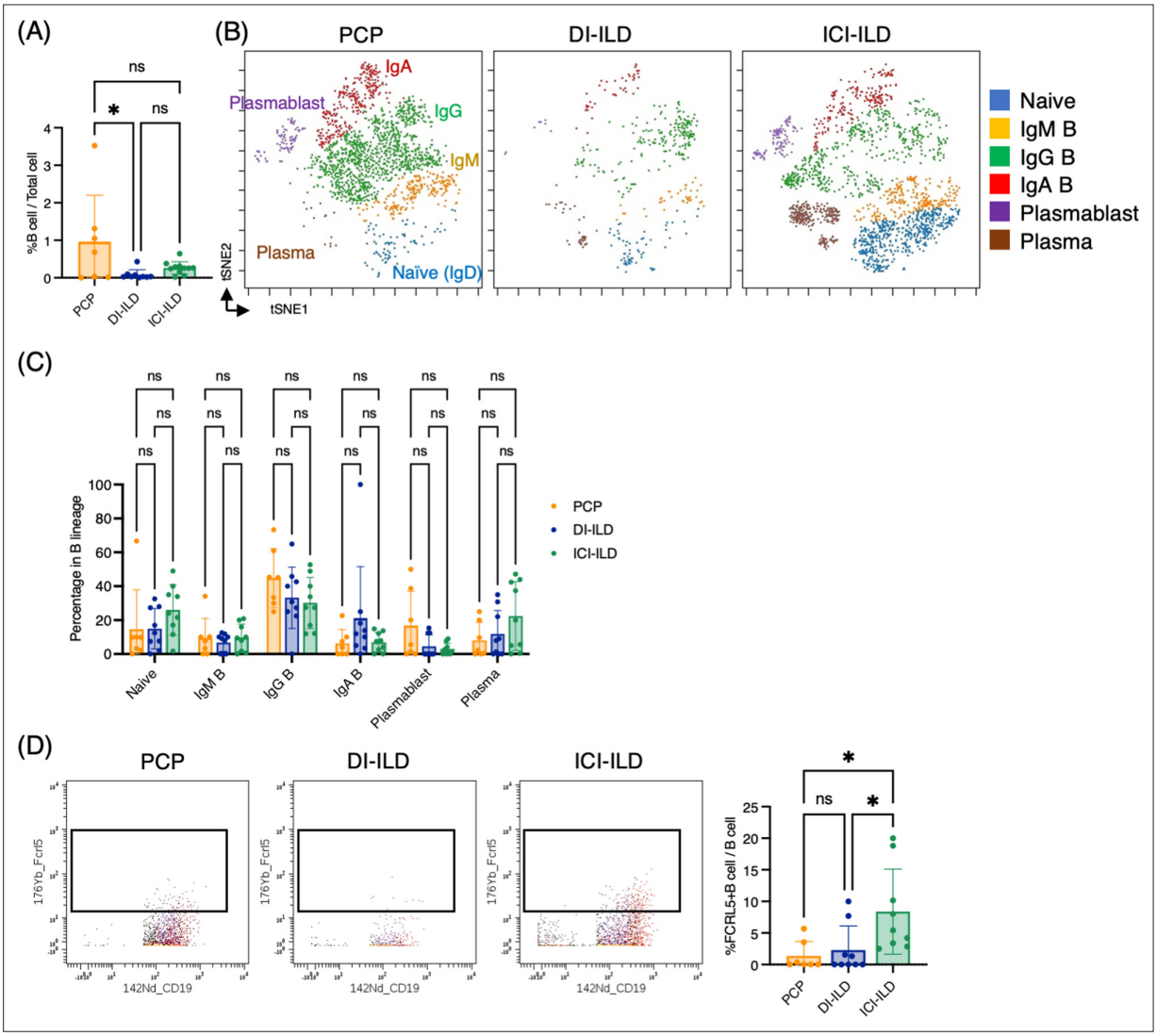

Figure 4. Characterization of B cell subsets in bronchoalveolar lavage fluid (BALF) from patients with *Pneumocystis jirovecii* pneumonia (PCP), cytotoxic drug-related interstitial lung disease (DI-ILD), and immune-checkpoint inhibitor-related ILD (ICI-ILD). (**A**) Percentages of B cells and plasma cells in $CD45^+$ BALF cells. (**B**) t-stochastic neighborhood embedding (t-SNE) plots of concatenated samples visualizing the distribution of B cell subpopulations in $CD64^-CD3^-$ and $CD19^+$ or $CD138^+$ gated B cells in BALF from patients with PCP, DI-ILD, and ICI-ILD. Naive B cells are defined by $CD19^+IgD^+$, IgM B cells: $CD19^+$ IgM^+, IgG B cells: $CD19^+$ IgG^+, IgA B cells: $CD19^+$ IgA^+, plasmablasts: $CD19^+$ $CD27^+$ $CD38^+$ $CD138^-$, plasma cells: $CD19^-$ $CD138^+$ and IgG^+ or IgA^+. (**C**) Percentages of B cell subpopulations in PCP (n = 7), DI-ILD (n = 9), and ICI-ILD (n = 9). Dot plots represent individual samples. (**D**) Two-dimensional dot plots depicting FCRL5-expressing B cells within a gated population of B cells defined as $CD64^-CD3^-$ and $CD19^+$ or $CD138^+$. Percentages of FCRL5-expressing B cells within the total B cell population are also shown.

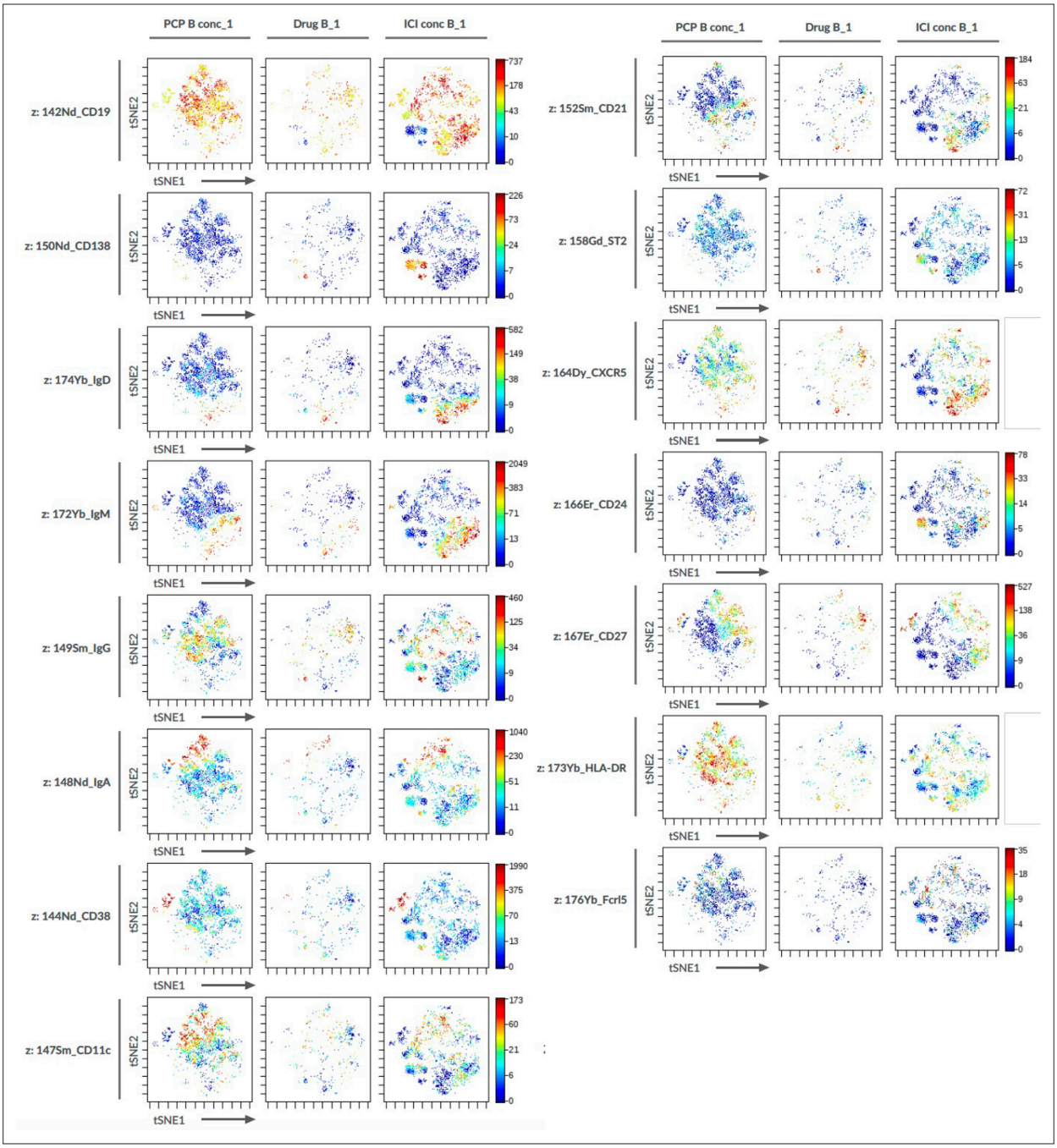

Figure 4—figure supplement 1. B cell marker expression on the t-stochastic neighborhood embedding (t-SNE) projection in ***Figure 4B***.

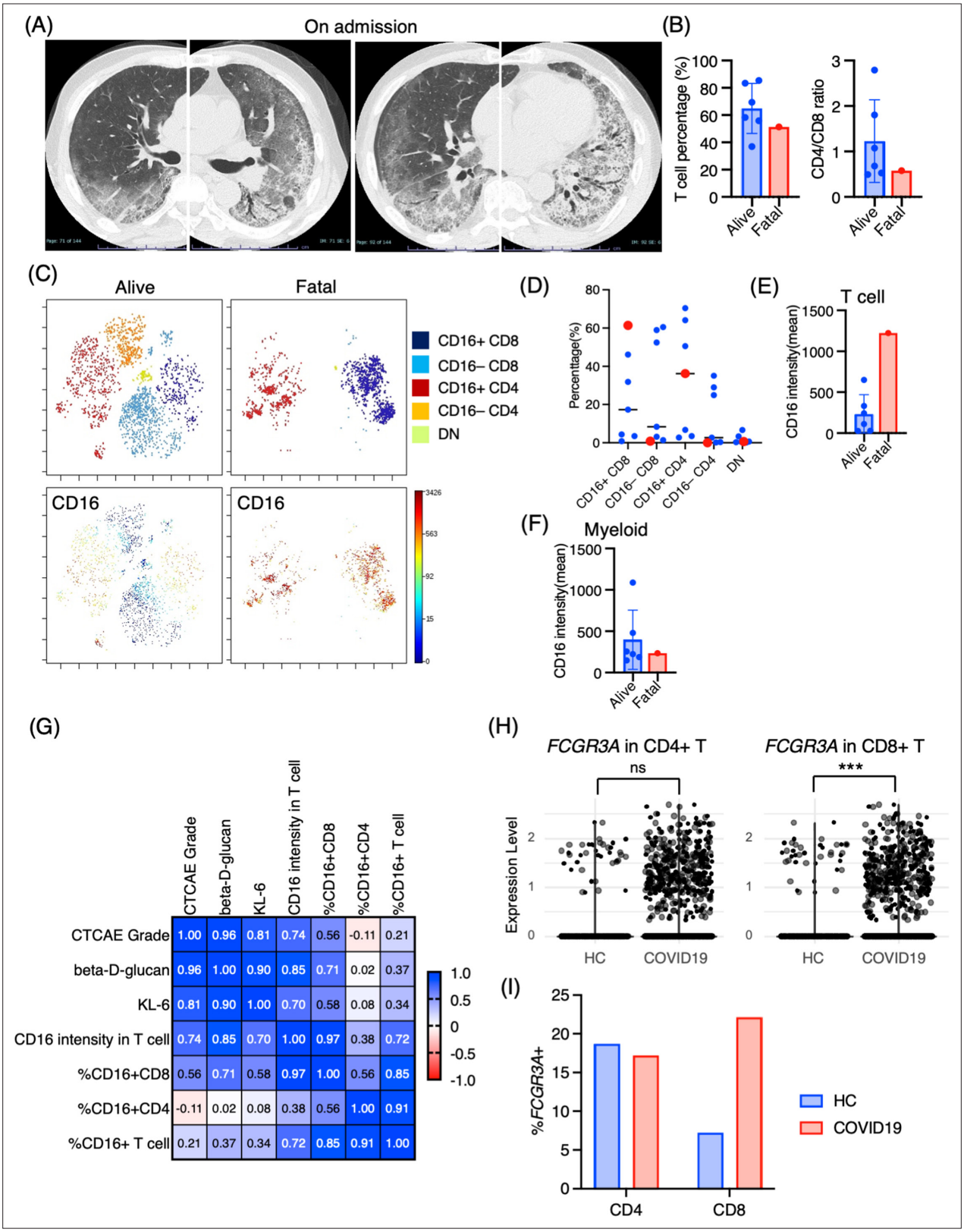

Figure 5. Immunological phenotypes in a fatal case of *Pneumocystis jirovecii* pneumonia (PCP). (**A**) Chest computed tomography images of the patient upon admission reveal the emergence of bilateral diffuse ground glass opacities and infiltration in both lungs. (**B**) Comparison of T cell percentage and CD4/CD8 ratio between a fatal case and surviving cases of PCP. (**C**) t-stochastic neighborhood embedding (t-SNE) plots illustrating the distribution of T cell subpopulations in bronchoalveolar lavage fluid (BALF) T cells (gated as $CD45^+CD2^+CD3^+$) from a fatal case and surviving cases of PCP. Double-

Figure 5 continued on next page

Figure 5 continued

negative (DN) T cells were defined as $CD4^{-}CD8^{-}$ T cells. (**D**) Percentages of each T cell subpopulation. Red dots represent the value of the fatal case. (**E**) Mean CD16 intensity in the T cell population. (**F**) Mean CD16 intensity in the myeloid cell population. (**G**) The correlation matrix in PCP cases. Pearson *r* values are shown in each square. (**H**) Violin plots illustrate *FCGR3A* (CD16) expression intensity on $CD4^{+}$ and $CD8^{+}$ T cells, with each dot representing an individual cell in BALF from healthy controls (HCs) and COVID-19 patients, derived from single-cell RNA-seq dataset GSE145926. The significance of differences was assessed using the Wilcoxon test. ns: not significant, ***p<0.001. (**I**) The proportion of *FCGR3A* (CD16)-positive cells within the $CD4^{+}$ and $CD8^{+}$ T cell populations in BALF from HC and COVID-19 patients, with the *FCGR3A* expression threshold set at 0.5.

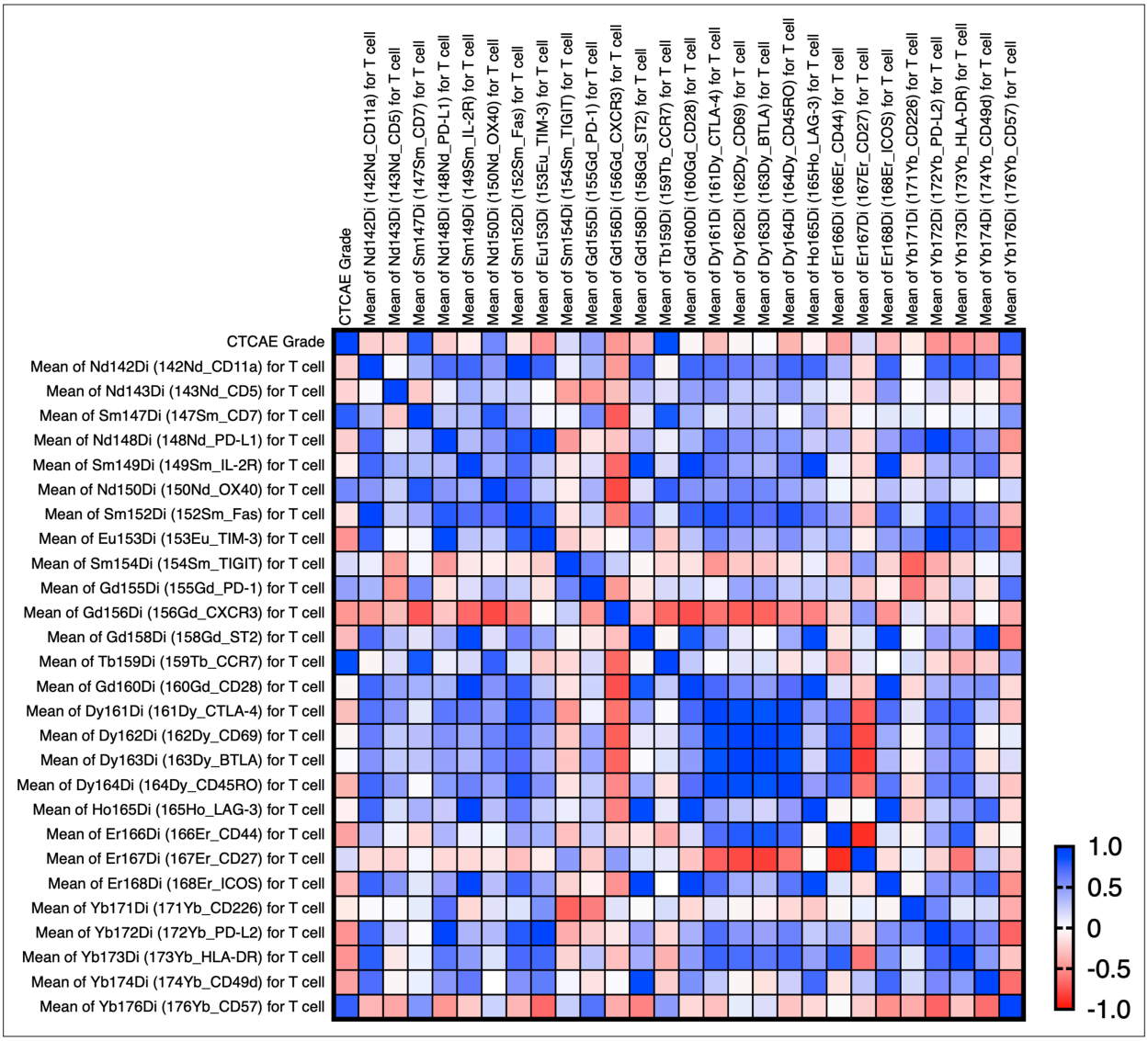

Figure 5—figure supplement 1. The correlation matrix with the CTCAE and intensity of each T cell markers in *Pneumocystis jirovecii* pneumonia (PCP) cases. The correlation was calculated using the Pearson correlation coefficient. This involved correlating the CTCAE grade directly with the mean expression levels of each marker. The computations were conducted using GraphPad Prism version 9. CCR7, CD7, and CD57 are correlated with the severity (CTCAE) of PCP (p-values: 0.009, 0.035, and 0.039, respectively).

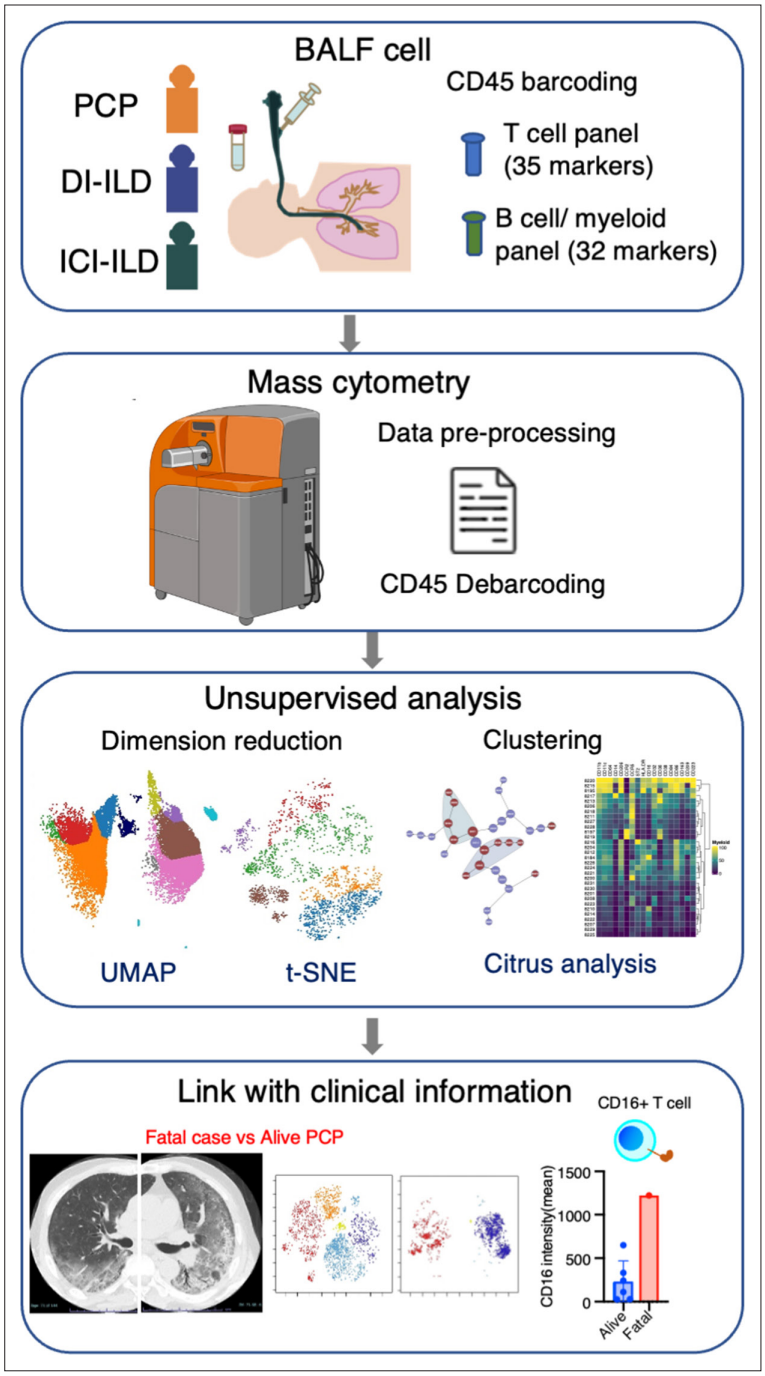

Figure 6. Graphical abstract of the study. Bronchoalveolar lavage fluid (BALF) samples were collected from patients with *Pneumocystis jirovecii* pneumonia (PCP), cytotoxic drug-induced interstitial lung disease (DI-ILD), and immune-checkpoint inhibitor-related ILD (ICI-ILD). Subsequently, BALF cells were analyzed using mass cytometry with a T cell panel (35 markers) and B cell/myeloid cell panel (32 markers) following CD45 barcoding for sample identification. The study found that there was a significant increase in the expansion of $CD16^{+}$ T cells in patients with PCP, with the highest CD16 expression observed in a fatal case of PCP.